Adaptive robotic CT trajectory selection: An object-dependent data-driven approach

Seungjun Yoo, Seokwon Oh, Junho Lee, Yoonsang Hong, Seongbin Bae, and Ho Kyung Kim*
Computational X-ray Imaging Laboratory, School of Mechanical Engineering, Pusan Nat'l Univ., Busandaehakro 63beon-gil, Busan 46241
**Corresponding author: hokyung@pusan.ac.kr*

***Keywords : Computed tomography, Robotic CT, Scan trajectory, Radon space**

1. Introduction

Recently, research on robotic computed tomography (CT) systems utilizing two multi-degree-of-freedom robotic arms equipped with an X-ray source and a detector has been actively conducted [1]. A key advantage of robotic CT is its ability to perform targeted scans on specific regions of large or geometrically complex objects, which are typically impossible to scan with conventional CT. Furthermore, by utilizing flexible scanning trajectories, these systems can selectively avoid or acquire specific projections, effectively mitigating various CT artifacts, such as metal and cone-beam artifacts.

The primary research areas in robotic CT can be broadly categorized into three domains: 1) image reconstruction, 2) geometric calibration, and 3) scan trajectory design [2]. Proper trajectory planning offers the significant benefit of employing scan paths specifically tailored to the target object and task. However, because the available scanning trajectories in a robotic CT system are practically infinite, an improperly configured path can severely degrade image quality. Therefore, selecting an optimal scanning trajectory is essential.

In this study, we propose a method to derive an object-specific scanning trajectory based on the Radon transform, the fundamental theory underlying CT image reconstruction. To achieve an optimal scanning path, prior information was extracted from the CAD data of the inspected object and subsequently utilized for trajectory optimization.

2. Methods and Materials

2.1 Theoretical background

To achieve high-resolution and sharp reconstructions of specific planes or edges of an inspected object in computed tomography, a fundamental geometric requirement is the acquisition of X-ray paths that pass tangentially to those edges [3]. To analyze this requirement mathematically, the spatial information of the object is transformed into a 3D Radon space. As illustrated in Fig. 1(a), this transformation process is defined by the following equation:

$$\mathcal{R}f(\mathbf{n}, s) = \int_{\mathbf{x}\in\mathbb{R}^3} f(\mathbf{x})\delta(\mathbf{n}^{\mathrm{T}}\mathbf{x} - s)d\mathbf{x}, \quad (1)$$

where $f(\boldsymbol{x})$ represents the spatial distribution function of the object, $\boldsymbol{n}$ is the unit normal vector to the plane, $\boldsymbol{x}$ denotes the spatial position vector in a three-dimensional space $\mathbb{R}^3$, and s indicates the perpendicular distance from the origin to the plane. From the acquisition perspective, when a projection view of a cone-beam CT system is transformed into the Radon domain, the geometrically sampled region forms the surface of a "spherical cap" governed by the cone-angle. The diameter of the sphere derived from this cap

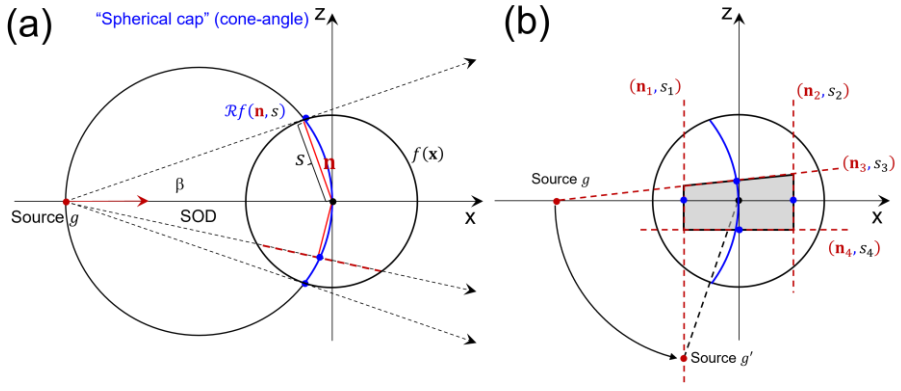

Fig. 1. Geometric representation of the 3D Radon transform and object-specific sampling. (a) Illustration of the 3D Radon transform and the formation of a "spherical cap" representing the sampled region for a given source position g with a specific SOD. (b) Mapping of an object's planar surfaces into discrete feature points (blue dots) in the Radon space. The schematic demonstrates how different X-ray source positions (g and g') optimally sample different subsets of the object's geometric features.

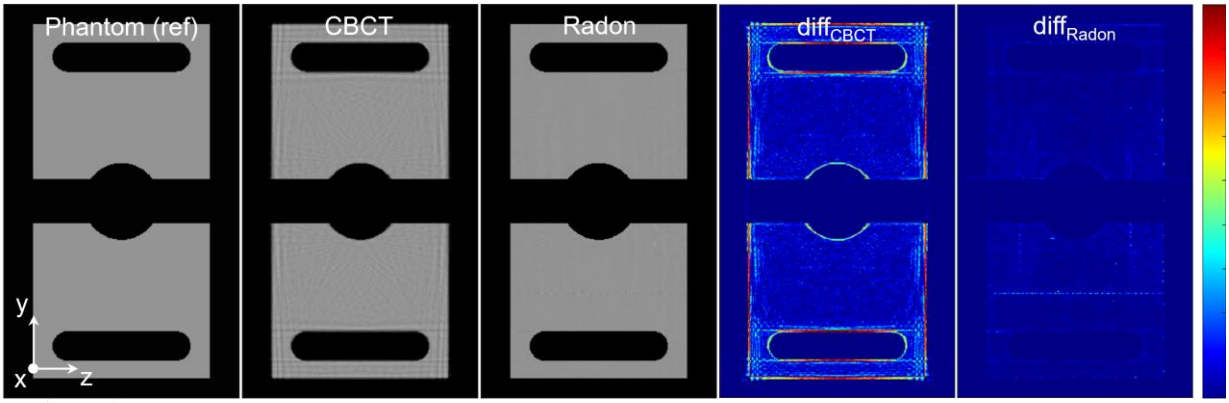

Fig. 2. Image reconstruction results and difference maps of the test phantom (a compressor sub-component). The difference maps (ΔV_{CBCT} and $\Delta V_{\mathrm{Radon}}$) visualize the absolute error compared to the reference phantom.

corresponds directly to the source-to-object distance (SOD).

Through this transformation, every planar surface existing in the spatial domain corresponds uniquely to a discrete point in the 3D Radon space, which is defined as a feature. Consequently, when the principal planes extracted from the object's CAD data are transformed, the object is effectively represented as a multitude of these feature points. As depicted in Fig. 1(b), the distinct faces of the object (e.g., defined by n_1, s_1) are mapped to specific discrete points (blue dots) in the Radon space.

Because the prior geometric information of the object is already known and mapped as features, it is possible to mathematically determine which specific regions in the Radon space are sampled by any given projection view. By altering the source position (e.g., from g to g'), the intersecting spherical cap changes, thereby allowing the system to sample different sets of object feature points.

2.2 Trajectory selection

To achieve high-resolution reconstruction with a minimal number of projections, the proposed algorithm is designed to maximize sampling coverage. First, structural information from the object's CAD data is mapped into the Radon space as discrete feature points, denoted as x_i. In this domain, the sampling region of a candidate cone-beam projection geometrically forms the surface of a spherical cap. A feature x_i is considered successfully sampled by a projection if its distance to the spherical cap falls within a permissible tolerance τ. This tolerance can be approximated as follows [4]:

$$\tau_i \approx |d_i| \frac{\pi}{m}, \tag{2}$$

where d_i represents the feature's distance from the origin in the Radon space, and m is number of pixels of detector.

Consequently, the optimal source position (projection view), g^*, is determined by identifying the spherical cap that maximizes the total number of sampled features:

$$g^* = \underset{g}{\operatorname{argmax}} \, \# \left\{ i \mid \left\| x_i - \frac{g}{2} \right\| \leq \tau \right\}, \tag{3}$$

where # indicates the total count of feature points satisfying the sampling condition. By iteratively solving this maximization problem, the algorithm extracts projection views with the highest scores.

2.3 Evaluation

To quantitatively validate the performance of the proposed algorithm, a MATLAB simulation was conducted to compare the reconstructed CT images from the optimized trajectory with those from a conventional circular trajectory. The image quality was assessed using three objective metrics. First, the overall reconstruction accuracy was measured using the root mean squared error (RMSE) of the object-only region, calculated as $\mathrm{RMSE} = \sqrt{\left(\frac{1}{N}\sum_{i=1}^{N}|V_i - V_{\mathrm{ref}}|\right)^2}$. Second, the Shannon entropy (SE) for the CT images was evaluated to assess the information content and clarity, defined as $\mathrm{SE} = -\sum_{i=1}^{N} p_i \log_2(p_i) / \log_2 N$, where N is the number of histogram bins and p_i represents the probability of the i-th intensity bin. Finally, the edge sharpness was evaluated using a figure of merit (FOM) based on the gradient of the edge region, expressed as $\mathrm{FOM} = \frac{1}{\Omega}\sum_{\mathbf{x}\in\Omega}\left|G_i(\mathbf{x}) - G_{ref}(\mathbf{x})\right|$. In this equation, G is the gradient magnitude defined as $G = \sqrt{G_x^2 + G_y^2 + G_z^2}$, and Ω denotes the edge-only region of interest consisting of voxels identified as edges.

3. Preliminary Results

To validate the proposed trajectory extraction algorithm, an open-source CAD model of a compressor sub-component was utilized as the test phantom. The image reconstruction was performed using the Simultaneous Algebraic Reconstruction Technique (SART) implemented via the TIGRE toolbox in MATLAB. The proposed Radon-based trajectory, utilizing 70 projections, was directly compared against a

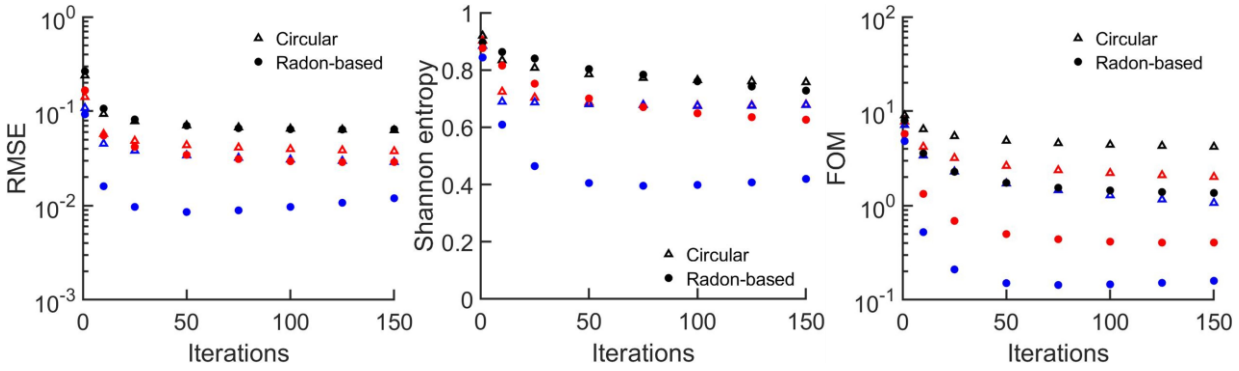

Fig. 3. Quantitative evaluation results as a function of the iteration number of SART. The performance of the conventional circular trajectory (72 projections) is compared with the proposed Radon-based trajectory (70, 42, and 14 projections) using RMSE, Shannon entropy, and an edge sharpness FOM. The marker colors denote the number of projections used: black represents 15 circular and 14 Radon-based projections; red indicates 45 circular and 42 Radon-based projections; and blue corresponds to 72 circular and 70 Radon-based projections.

conventional circular trajectory consisting of 72 projections.

Visual comparisons of the reconstructed images clearly demonstrate the superiority of the proposed method, as shown in Fig. 2. The difference maps calculated against the reference phantom, where red indicates high error magnitudes, reveal that the conventional circular trajectory suffers from large deviations, particularly along the boundary edges of the object. In contrast, the Radon-based trajectory exhibits uniformly minimal errors across the entire region, successfully preserving the geometric edge structures.

Quantitative evaluations further support these visual findings, as illustrated in Fig. 3. The performance metrics—RMSE, SE, and FOM—were analyzed as a function of the iteration number across different projection counts. The Radon-based method significantly outperformed the circular trajectory across all metrics. Notably, the proposed method achieved equivalent RMSE and SE scores using only 42 projections (red circles) compared to the 72 projections required by the circular trajectory (blue triangles). Furthermore, in terms of FOM, the Radon-based trajectory with merely 14 projections (black circles) demonstrated performance comparable to the 72-projection circular scan (blue triangles). These results highlight the exceptional efficiency of the proposed object-dependent trajectory in few-view CT scenarios.

4. Conclusion

In this study, we proposed an object-dependent scan trajectory optimization method based on the 3D Radon transform for few-view CT applications. The simulation results demonstrated that the proposed Radon-based trajectory significantly outperforms the conventional circular trajectory, effectively preserving edge structures with a highly reduced number of projections. Further details regarding the trajectory extraction algorithm and comprehensive quantitative analyses will be presented at the conference. Future research will focus on the experimental validation of the proposed approach. Moreover, we plan to extend the trajectory optimization method to account for physically unscannable regions caused by the kinematic constraints and limited accessibility of the actual robotic CT system.

ACKNOWLEDGEMENTS

This work was supported by the National Research Foundation of Korea (NRF) grant funded by the Korea government (MSIT) (RS-2024-00340520).

REFERENCES

[1] W. Holub, F. Brunner, and T. Schön, RoboCT application for in-situ inspection of join technologies of large scale objects, International Symposium on Digital Industrial Radiology and Computed Tomography, 2019.
[2] G. Herl, S. Wittl, A. Jung, N. Handke, A. Weiss, M. Eberhorn, et al., RoboCT: The state and current challenges of industrial twin robotic CT systems, Sensors, Vol. 25, No. 10, 3076, 2025.
[3] E. T. Quinto, “Singularities of the X-ray transform and limited data tomography in R^2 and R^3,” SIAM Journal on Applied Mathematics, Vol. 24, No. 5, pp. 1215-1225, 1993.
[4] M. Linde, W. Wiest, A. Trauth, and M. G.R. Sause, Trajectory optimization for few-view robot-based CT: Transitioning from static to object-specific acquisition geometries, Tomography of Materials and Structures, Vol. 7, 100058, 2025